





The anticancer effect of mebendazole may be due to M1 monocyte/macrophage activation via ERK1/2 and TLR8-dependent inflammasome activation

Kristin Blom, Wojciech Senkowski, Malin Jarvius, Malin Berglund, Jenny Rubin, Lena Lenhammar, Vendela Parrow, Claes Andersson, Angelica Loskog, Mårten Fryknäs, Peter Nygren & Rolf Larsson

To cite this article: Kristin Blom, Wojciech Senkowski, Malin Jarvius, Malin Berglund, Jenny Rubin, Lena Lenhammar, Vendela Parrow, Claes Andersson, Angelica Loskog, Mårten Fryknäs, Peter Nygren & Rolf Larsson (2017): The anticancer effect of mebendazole may be due to M1 monocyte/macrophage activation via ERK1/2 and TLR8-dependent inflammasome activation, *Immunopharmacology and Immunotoxicology*, DOI: [10.1080/08923973.2017.1320671](https://doi.org/10.1080/08923973.2017.1320671)

To link to this article: <http://dx.doi.org/10.1080/08923973.2017.1320671>

 View supplementary material 

 Published online: 04 May 2017.


 Submit your article to this journal 

 Article views: 2

 View related articles 

 View Crossmark data 

The anticancer effect of mebendazole may be due to M1 monocyte/macrophage activation via ERK1/2 and TLR8-dependent inflammasome activation

Kristin Blom^a, Wojciech Senkowski^a, Malin Jarvius^a, Malin Berglund^a, Jenny Rubin^a, Lena Lenhammar^a, Vendela Parrow^a, Claes Andersson^a, Angelica Loskog^b, Mårten Fryknäs^a, Peter Nygren^b and Rolf Larsson^a 

^aDepartment of Medical Sciences, Division of Cancer Pharmacology and Computational Medicine, Uppsala University, Uppsala, Sweden;

^bDepartment of Immunology, Genetics and Pathology, Science for Life Laboratory, Uppsala University, Uppsala, Sweden

ABSTRACT

Mebendazole (MBZ), a drug commonly used for helminthic infections, has recently gained substantial attention as a repositioning candidate for cancer treatment. However, the mechanism of action behind its anticancer activity remains unclear. To address this problem, we took advantage of the curated MBZ-induced gene expression signatures in the LINCS Connectivity Map (CMap) database. The analysis revealed strong negative correlation with MEK/ERK1/2 inhibitors. Moreover, several of the most upregulated genes in response to MBZ exposure were related to monocyte/macrophage activation. The MBZ-induced gene expression signature in the promyeloblastic HL-60 cell line was strongly enriched in genes involved in monocyte/macrophage pro-inflammatory (M1) activation. This was subsequently validated using MBZ-treated THP-1 monocytoic cells that demonstrated gene expression, surface markers and cytokine release characteristic of the M1 phenotype. At high concentrations MBZ substantially induced the release of IL-1 β and this was further potentiated by lipopolysaccharide (LPS). At low MBZ concentrations, cotreatment with LPS was required for MBZ-stimulated IL-1 β secretion to occur. Furthermore, we show that the activation of protein kinase C, ERK1/2 and NF-kappaB were required for MBZ-induced IL-1 β release. MBZ-induced IL-1 β release was found to be dependent on NLRP3 inflammasome activation and to involve TLR8 stimulation. Finally, MBZ induced tumor-suppressive effects in a coculture model with differentiated THP-1 macrophages and HT29 colon cancer cells. In summary, we report that MBZ induced a pro-inflammatory (M1) phenotype of monocytoic cells, which may, at least partly, explain MBZ's anticancer activity observed in animal tumor models and in the clinic.

ARTICLE HISTORY

Received 13 November 2016
Revised 4 April 2017
Accepted 15 April 2017

KEYWORDS

Repositioning; cancer therapy; monocytes; macrophages; mebendazole

Introduction

Mebendazole (MBZ) is an antiparasitic agent that is clinically used for the treatment of various forms of helminthic diseases. It has also been reported in numerous studies to possess anticancer activity and repositioning potential as a cancer drug, as it has shown striking activity in several cancer models both *in vitro* and *in vivo*^{1–11}. Moreover, MBZ has demonstrated activity in the clinical setting producing objective tumor responses in therapy-resistant and refractory cancer patients^{12,13}.

The antitumor activity of MBZ has been primarily attributed to its ability to inhibit tubulin^{3,4}, but other mechanisms, including protein kinase inhibition⁷, antiangiogenesis^{6,9}, proapoptotic activity^{2,8} and inhibition of the Hedgehog pathway¹⁴ have also been suggested. Notably, MBZ appears to differ from other clinically used benzimidazole drugs in several respects. For example, in a glioma orthotopic models, MBZ, but not the clinically approved benzimidazole albendazole (ABZ), demonstrated *in vivo* efficacy despite being equally active *in vitro*³. Moreover, ABZ and another clinically used benzimidazole, fenbendazole (FBZ), did not show *in vivo* efficacy in these models even when tested at higher

doses than MBZ¹⁵. We have also previously shown that MBZ, but not ABZ, can potently inhibit a range of protein kinases⁷. Thus, more detailed knowledge on the MBZ anticancer mechanisms of action is needed.

For this purpose, we took advantage of the LINCS database resource (www.lincscloud.org) using its validated MBZ-induced gene signatures. The correlation analysis and gene set enrichment analysis suggested monocyte and macrophage activation. Using the monocytoic cell line model THP-1 monocytes we subsequently demonstrated that MBZ-induced gene expression, cytokine release and surface marker profiles typical of the pro-inflammatory M1 phenotype. Moreover, MBZ-induced IL-1 β release was dependent on NLRP3 inflammasome and TLR8 activation. These data suggest that MBZ can support M1 activation, which in turn may contribute to the anticancer activity observed *in vivo*.

Methods

Cell culture

Monocytoic THP-1 cells were obtained from ATCC (Manassas, VA) and were cultured in RPMI-1640 medium, supplemented

with 10% heat-inactivated fetal bovine serum (HIFBS), 2 mM L-glutamine, 100 U/100 µg/mL penicillin/streptomycin and 0.05 mM 2-mercaptoethanol (all from Sigma, St Louis, MO). All cell lines were cultured at 37 °C in a humidified atmosphere containing 5% CO₂. The human colorectal carcinoma cell line, HT-29 GFP, constitutively expressing green fluorescent protein (GFP), was obtained from Anticancer, Inc., (San Diego, CA) and was cultured in McCoy 5A medium, supplemented with 10% HIFBS, 2 mM glutamine, 100 µg/mL streptomycin and 100 U/mL penicillin (Sigma). Recombinant P2X7-overexpressing HEK293 cells were obtained from B'SYS GmbH (Witterswil, Switzerland) and cultured in DMEM F-12 HAM medium with 10% HIFBS, 100 U/100 µg/mL penicillin/streptomycin, 5 mM L-glutamine and 100 µg/mL G-412 sulfate (all from Sigma). All other reporter cell lines were purchased from InvivoGen (San Diego, CA). THP1-defNLRP3 cells have reduced NOD-like receptor pyrin domain containing 3 (NLRP3) inflammasome activity (used to study the involvement of NLRP3 in response to a given signal) and THP1-Null cells (control cell line) expressing high levels of NLRP3, ASC and pro-caspase-1. HEK-BlueTM-hTLR7 and -hTLR8 cells were obtained by co-transfection of the human TLR7 or TLR8 gene and an optimized SEAP (secreted embryonic alkaline phosphatase) reporter gene into HEK293 cells. The SEAP gene is placed under the control of the IFN-β minimal promoter fused to five NF-kappaB and AP-1-binding sites. Stimulation with a TLR ligand activates NF-kappaB and AP-1, which induce the production of SEAP. HEK-BlueTM-mTLR4 cells were obtained by cotransfection of the murine TLR4, MD-2 and CD14 coreceptor genes and an inducible SEAP reporter gene into HEK293 cells. All reporter cell lines including their corresponding parental counterparts were cultured strictly according to the manufacturer's instructions. All cell lines were cultured at 37 °C in a humidified atmosphere containing 5% CO₂.

Materials

MBZ, ABZ, FBZ, A740003 (P2X7 inhibitor), BzATP, lipopolysaccharide (LPS), interferon gamma (IFN γ), IL13 and IL4 were purchased from Sigma. The TLR7/8 agonists (R848, CL075 and imiquimod) were obtained from InvivoGen (San Diego, CA). The TLR8 agonist Motilimod was purchased from Selleckchem (Houston, TX). The compounds were kept as 10 mM stock solutions in dimethyl sulfoxide (DMSO, Sigma, St. Louis, MO) or sterile water and further diluted with culture medium (Sigma or ATCC) as needed. All other inhibitors and stimulants used were obtained from Sigma.

Bioinformatic analysis using the LINCS L1000 platform

The drug-induced gene expression perturbations of MBZ were studied using the public LINCS Connectivity Map (CMap) resource (www.lincscloud.org) that contains a collection of hundreds-of-thousands of L1000 gene-expression profiles from cells grown in monolayer exposed to a large numbers of small-molecule and genetic perturbagens (www.lincscloud.org). Since MBZ is present in the database, the

gene expression can be compared with other drugs and perturbagens. Score and ranking were retrieved from the LINCS CMap database using default settings (best 4 cell lines). Gene expression data for the HL-60 cell line was extracted from the Nextbio gene expression repository¹⁶ and subsequently uploaded to the LINCS query application. The query was based on genes (probes) with 2-fold up- (31 probes) or downregulation (70 probes) after exposure to MBZ. THP-1 gene expression data obtained using the Affymetrix U133 chip were uploaded and analyzed in a similar manner. Gene enrichment analysis was performed by the phenotype 4 ontology in the LINCS Canvas Browser application.

Measurement of cell viability

The Fluorometric Microculture Cytotoxicity Assay, FMCA, described in detail previously¹⁷, was used for measurement of the cytotoxic effect of library compounds and established standard drugs. The FMCA is based on measurement of fluorescence generated from hydrolysis of fluorescein diacetate (FDA) to fluorescein by cells with intact plasma membranes. Cells were seeded in 384-well plates using the pipetting robot Biomek 4000 (Beckman Coulter Inc., Brea, CA) and cultured overnight before drugs were added by the Echo Liquid Handler 550 system (Labcyte, Sunnyvale, CA). The number of cells seeded per well was 2500–5000, adjusted individually for each cell line. In each plate, four columns without drugs added served as controls and one column with medium only served as blank.

Measurement of phosphoprotein and cytokines

The levels of phosphoproteins, cytokines and chemokines were measured using the Luminex/MAGPIX system and commercially available kits for various analytes (Biorad). The assay is based on binding of the target of interest via antibodies to magnetic beads. The target is detected using biotinylated antibodies with a fluorescent reporter. The assays were performed according to the manufacturer instructions. Briefly, for the cytokine assay, the supernatant samples were incubated first with beads, then with detection antibody and finally with streptavidin-PE. The fluorescence was measured using the MagPix instrument (BioRad) and the concentration levels were calculated by fitting a standard curve. For the phosphoprotein assay, the protein concentrations in the lysates were first determined using a Micro-BCA method to ensure equal amounts of samples in the assay and then performed using the same protocol as in the cytokine assay. Protein detection was also performed using the WesTM—an automated western blotting system (ProteinSimple, San Jose, CA), which utilizes capillary electrophoresis-based immunodetection. WesTM reagents were obtained from the manufacturer and used according to their recommendations. Briefly, equal amounts of protein (2 µg) were added to the assay reagents, gently mixed, and then denatured at 95 °C for 5 min. Denatured samples, a biotinylated ladder, antibody diluent, primary antibodies, HRP-conjugated secondary antibodies, chemiluminescent substrate, and wash buffer were

dispensed to designated wells in a Wes™ microplate. The electrophoresis and immunodetection in the capillaries were fully automated and the data analyses were performed using the Compass software (Protein Simple), which also produce “virtual blot” images.

Measurement of M1 and M2 surface marker expression

THP-1 cells were incubated for 24 h in a 6-well plate (1×10^6 cells/well) with the corresponding stimuli (LPS 100 ng/mL, MBZ 10 μ M and control, respectively). The cells were then washed with cell culture media and then left for additional 24 h before they were detached using Accutase (Sigma) and washed with PBS. The cell suspension was then mixed with the conjugated antibodies CD86-PC7/CD86-AF750 and CD206-PB (Beckman Coulter), incubated for 15 min, washed with PBS (Sigma) and then analyzed on a Navios flow cytometer (Beckman Coulter). The data were then analyzed with the Kaluza software (Beckman Coulter) to determine the M1 and M2 polarization.

Measurement of gene expression markers in THP-1 cells

RNA from cell cultures was isolated using RNeasy Mini Kit from Qiagen, immediately frozen and stored at -70°C until further use. RNA purity and quality was measured using an ND 1000 spectrophotometer (NanoDrop Technologies, Wilmington, DE) and Bioanalyzer 2100 (Agilent Technologies Inc, Palo Alto, CA), respectively. Starting from 2 μ g of total RNA, gene expression analysis was performed using Genome U133 Plus 2.0 Arrays according to the GeneChip Expression Analysis Technical Manual (Rev. 5, Affymetrix Inc., Santa Clara, CA). Raw data was normalized using MAS5 (Affymetrix Inc., Santa Clara, CA).

For the L1000 assay, drugs and tool compounds were transferred to monolayer plates using Echo Liquid Handler 550 (Labcyte). Following 1- or 6-h incubation, the cell-culture medium was aspirated and cell lysis buffer (Genometry, Inc., Cambridge, MA) added. After 30-min incubation at room temperature, cell samples were mixed. Homogeneous lysates were transferred to 384-well plates (Nunc) and frozen at -70°C . Lysates were processed, and the resulting gene-expression data subjected to a panel of quality control tests, performed by Genometry in their facility (www.genometry.com). The L1000 expression profiles delivered were scaled, normalized and log transformed, and denominated in the Affymetrix HG-U133A feature space.

Measurement of NF-kappaB activation

Compounds were plated in duplicates in 96-well, clear, flat-bottom plates (Nunc) at 10x the final concentration in culture medium containing 3% DMSO (0.3% final concentration). HEK-Blue™-hTLR7 and -hTLR8 cells, HEK-Blue™-mTLR4 cells and their corresponding parental counterparts were suspended in HEK-Blue™-Detection medium (InvivoGen, prepared accordingly to manufacturer's instructions) and seeded at 40,000, 25,000 and 50,000 cells/well, respectively, in the

compound-containing plates and incubated at 37°C , 5% CO_2 for 24 h. The SEAP activity was measured by reading the optical density at 650 nm with a FlexStation 3 (Molecular Devices, Sunnyvale, CA).

Measurement of cytoplasmic calcium

Cytoplasmic calcium was assayed in THP-1 cells and HEK293 cells stably expressing the P2X7 receptor. These cells were plated in their culture medium (without 2-mercaptoethanol for the THP-1 cells) at 80,000 cells/well in 96-well, black, clear-bottom plates (PerkinElmer, Waltham, MA) and incubated at 37°C , 5% CO_2 overnight. Changes in cytoplasmic calcium in response to test compounds were assessed the next day using the Fluo-4 Direct™ Calcium Assay Kit (Molecular Probes™). On the day of assay, an equal volume of $2 \times$ Fluo-4 Direct™ calcium reagent loading solution (10 mL Fluo-4 Direct™ calcium assay buffer and 200 μ L 250 mM probenecid to one bottle of Fluo-4 Direct™ calcium reagent) was added directly to the wells containing cells in culture medium. The cells were incubated with the dye at 37°C for 30 min followed by 30-min incubation in room temperature. Test compounds were evaluated in duplicates. They were added to cells at 5x final concentration in culture medium, containing 1.5–2.5% DMSO (0.3–0.5% final concentration). The effect of test compound on cytoplasmic calcium was determined with a FlexStation 3 (Molecular Devices, Sunnyvale, CA) set for bottom read with 485 nm excitation and 525-nm emission wavelengths and a 515 nm emission cutoff. Data were captured using SoftmaxPro (Molecular Devices), and max-min was used to calculate the change in fluorescence intensity.

Measurement of tubulin polymerization

Tubulin polymerization from purified tubulin monomers was measured as increased fluorescence because of the incorporation of a fluorescent reporter into growing microtubules. All reagents necessary for performing the assay were provided in the kit BK011 from Cytoskeleton (Denver, CO). The fluorescence was measured at 1-min interval for 60 min using a FLUOstar Optima (BMG Labtech GmbH, Offenburg, Germany).

Measurement of anticancer activity

For differentiation and polarization of THP-1 cells to macrophages, 25 ng/mL PMA, 20 ng/mL $\text{IFN}\gamma$, 100 ng/mL LPS, 20 ng/mL IL-4 and 20 ng/mL IL-13 (final concentrations) were used according to an established protocol with minor modifications¹⁸. MBZ was used at 1 and 10 μ M. All solutions were made in RPMI-1640 medium with no β -mercaptoethanol added. First, PMA was added to 500,000 THP-1 cells seeded into each of the wells of a 12-well plate (Corning). The plate was placed for monitoring in an Incucyte ZOOM reader (Essen Bioscience, UK), capturing nine images of each well at 2-h interval. After 30 h, LPS/ IFN (M1), IL-4/IL-13 (M2), DMSO (control) and MBZ were added to separate wells. DMSO was added in a concentration corresponding to that of added

Table 1a. Negative connectivity map scores for the mebendazole signature (best4).

Rank (n = 3273)	Compound name	Mechanism	Correlation score
3273	PD-0325901	Mek/Erk inhibition	-99.55
3272	PD-0325901	Mek/Erk inhibition	-99.1
3271	PD-98059	Mek/Erk inhibition	-98.3
3270	U0126	Mek/Erk inhibition	-97.9
3269	Selumetinib	Mek/Erk inhibition	-97.9
3268	Verapamil	Calcium channel	-97.8
3267	AS-605240	Mek/Erk inhibition	-97.7
3266	PP-2	Src inhibition	-96.9
3265	AS-703026	Mek/Erk inhibition	-96.7
3264	U-0126	Mek/Erk inhibition	-96.6
3263	RHO-kinase inhibitor-III	Rho-kinase inhibition	-96.5
3262	10-DEBC	Akt/Pkb	-95.7
3261	ERK-inhibitor-11E	Mek/Erk inhibition	-95.6
3260	Forskolon	c-AMP activation	-95.5
3259	PD-184352	Mek/Erk inhibition	-95.4

Table 1b. Overexpression connections for the mebendazole signature (best4).

Rank	Gene name	Correlation score
1	LPAR1	99.5
2	CRK	98.4
3	MAGEB6	98.1
4	TRAF2	96.7
5	BCL10	94.4
6	LTBR	91.9
7	CD40	90.7
8	RELB	90.3

MBZ. The plate was once again monitored and photographed in the Incucyte ZOOM reader. After another 18 h, the plate was centrifuged at 200 *g* for 5 min and the stimulant-containing medium was removed. The cell pellets were resuspended in 500 μ L of fresh medium and replaced in the original wells of the plate. Subsequently, 100,000 of HT-29/GFP cells were added into each well in 500 μ L of fresh medium. For monitoring and analysis, the plate was placed in the Incucyte ZOOM, using phase-contrast and the green fluorescence filters.

Data analysis and statistics

Concentration-response data were analyzed using GraphPad Prism6 (GraphPad Software Inc., San Diego, CA). Data were processed using non-linear regression to a standard sigmoidal dose-response model to obtain IC₅₀-values (the concentration resulting in 50% growth inhibition). Statistical analysis was performed using the Students t-test module in GraphPadPrism.

Results

To characterize MBZ's mechanism of action, we took advantage of the LINCS database resource. LINCS database is a collection of hundreds-of-thousands compound-induced gene expression profiles from wide range of cell types (<http://lincscloud.org>). For the analysis, we used the default curated MBZ signatures. Using the CMap feature of LINCS database, we used the MBZ signature as a query to identify compounds that induce similar gene expression signature. As a result, we observed a strong negative correlation to multiple MEK/ERK1/2 inhibitors (Table 1(a)). This enrichment was MBZ-

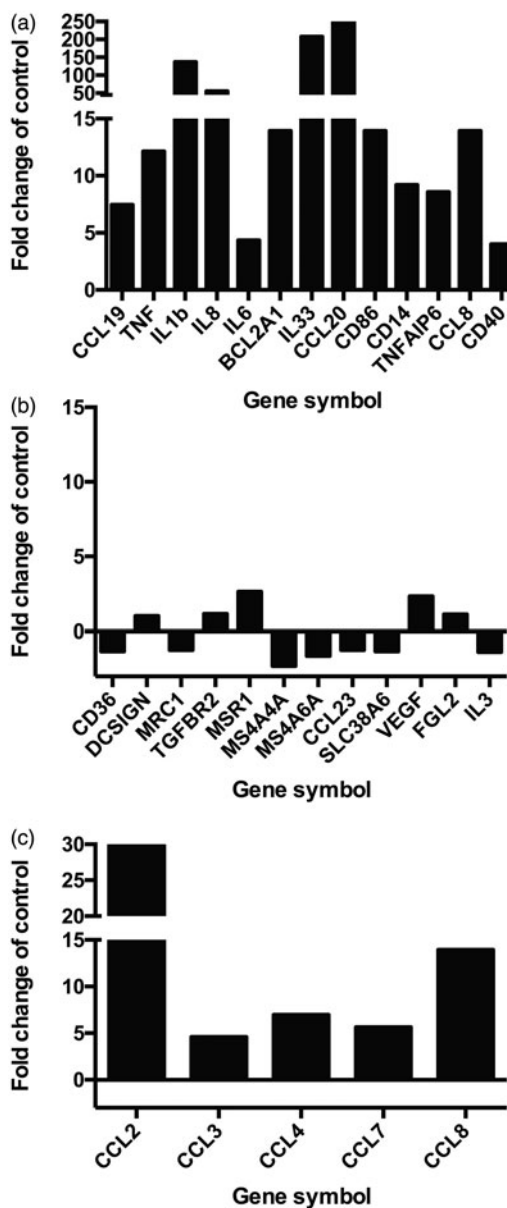


Figure 1. Gene expression analysis of THP-1 cells in response to 10 μ M MBZ using the U338 array. In (a) and (b) genes were selected by the classification of Stewart et al.¹⁸ for M1 and M2 phenotypes, respectively. Results are presented as fold-change versus DMSO-treated control. (c) Expression of genes encoding T-cell-attracting chemokines after treatment with 10 μ M MBZ. MBZ clearly increased cytokines and chemokines associated with the M1 phenotype.

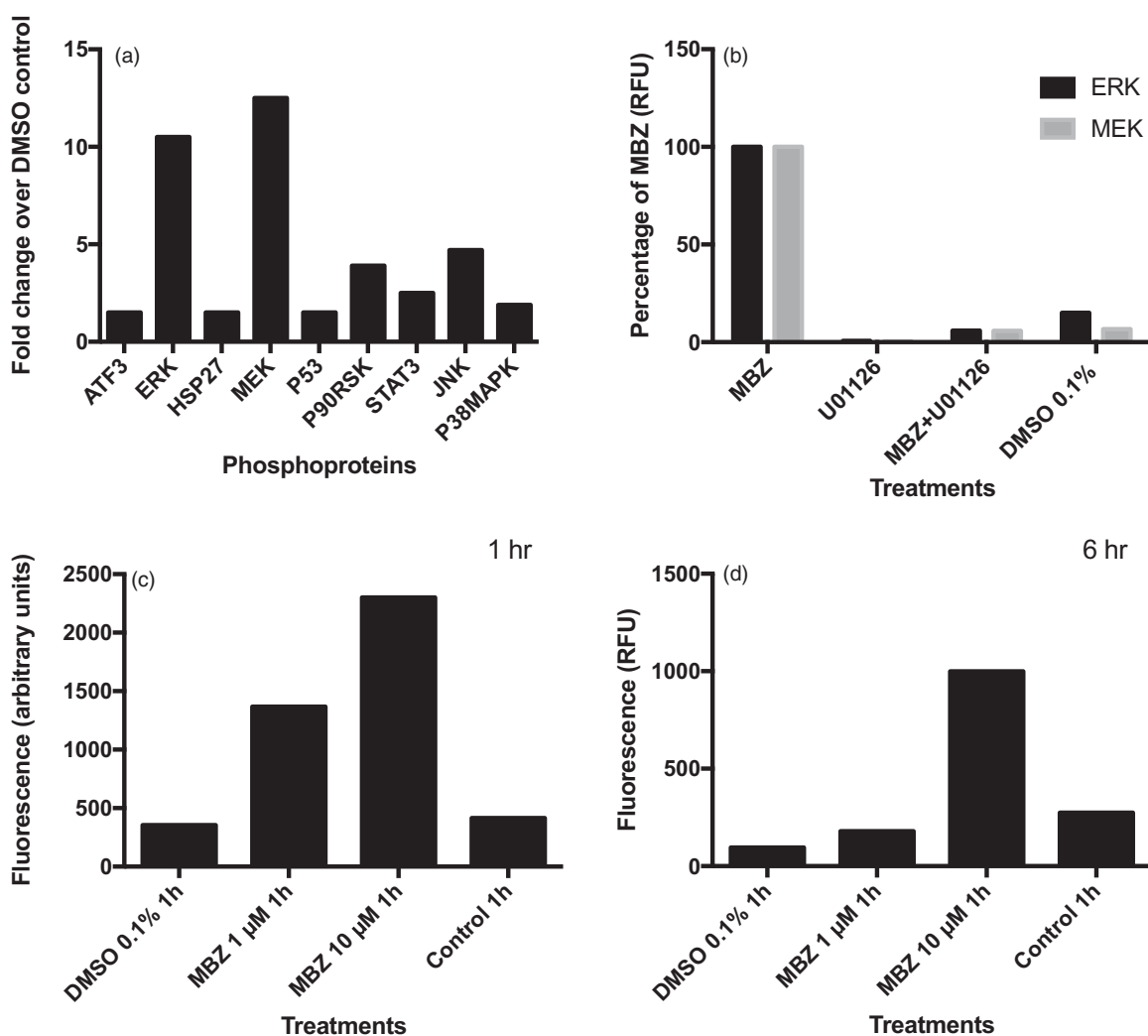


Figure 2. Effect of MBZ (10 μ M) on phosphoprotein activation in THP-1 cells. (a) The response to MBZ (10 μ M) is shown for the MAPK panel of phosphoproteins. (b) MBZ-(10 μ M)-induced activation of MEK and ERK is shown with and without addition of the MEK inhibitor U0126 (10 μ M). In (c) and (d) the response after 1 or 6 h of MBZ exposure, respectively, are shown. MBZ induced a pronounced increase in MEK and ERK1/2 phosphorylation which could be inhibited by the MEK inhibitor U0126.

specific and not shared by other benzimidazoles or tubulin inhibitors (Supplemental Figure 1). These results indicated that MBZ-induced ERK1/2 activation. We subsequently confirmed this by western blotting using the MCF7 cell line, in which MBZ induced the phosphorylation of ERK1/2 (not shown). Interestingly, we also found that the genes, overexpression of which resulted in gene-expression changes similar to those induced by MBZ (i.e. TRAP2, CD40 and LTBR), were related to monocyte activation¹⁹ (Table 1(b)). Enrichment analysis of the MBZ-induced MCF7 gene-expression signature, performed in the LINCS Canvas Browser tool, revealed enrichment with genes associated with immune stimulation and monocyte/macrophage activation (Supplemental Table 1).

Subsequently, similarly to the previous approach with MCF7 cells, we queried CMap using the MBZ signatures of the leukemic cell line HL60 (obtained from the Nextbio gene expression repository). We again identified strong negative connections to ERK1/2 inhibitors and enrichment in genes associated with monocyte/macrophage activation (Supplemental Table 2). Notably, in this cell line, we also found strong positive correlation to several protein kinase C (PKC)

activators (Supplemental Table 2). Indeed, PKC activators are known to induce THP-1 adherence and differentiation through an ERK-mediated mechanism²⁰. When investigating the individual genes, expression of cytokine-encoding genes associated with M1, but not the M2, phenotype of monocytes and macrophages¹⁸ was strongly upregulated (Supplemental Figure 2).

Based on these findings, we selected the THP-1 cell line, a well-characterized model of monocyte to dendritic cells (DC)/macrophage differentiation and activation, for further experiments²¹. Exposure of THP-1 cells for 6 h to 10 μ M MBZ resulted in strong upregulation of pro-inflammatory M1 phenotype genes encoding cytokines such as IL-1 β , TNF, IL8 and IL6, whereas little or no upregulation was observed for M2 markers including IL10 and VEGF (Figure 1(a,b)). The M1/M2 gene annotation was done according to Stewart et al.¹⁸. Also, the expression of genes encoding several pro-inflammatory, T-cell-attracting chemokines, including MCP-1 (CCL2), MIP-1a (CCL3) and MIP-1B (CCL4), was upregulated by MBZ (Figure 1(c)). Furthermore, MBZ pronouncedly induced MEK/ERK activation in THP-1 cells with little effect on other MAPK-

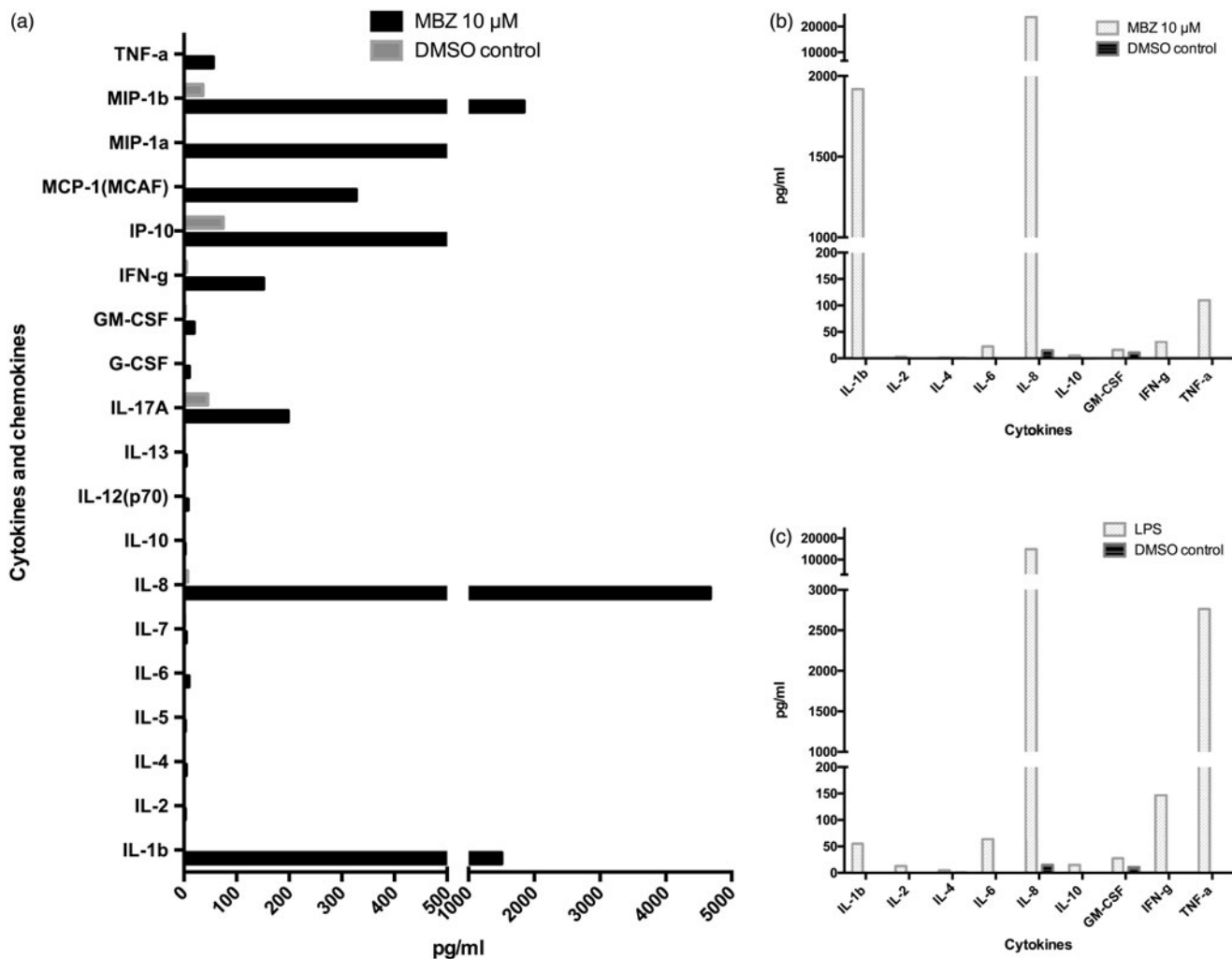


Figure 3. (a) Cytokine and chemokine release from THP-1 cells in response to 24-h exposure to MBZ. In (b) and (c) cytokine release for 9 selected cytokines in MBZ- or LPS-treated THP-1 cells, respectively, are shown. The measurements were repeated three times with similar results. The differences between MBZ (10 μM) and DMSO control for IL-1β, IL-6 and TNF were highly significant ($p < .001$, $n = 3$, Student's *t*-test).

related phospho-proteins (Figure 2(a)). The MEK inhibitor U0126 was able to abrogate this effect confirming that MEK is responsible for ERK1/2 phosphorylation (Figure 2(b)). ERK1/2 activation was more pronounced after MBZ exposure for 1 h (Figure 2(c)) compared with the 6-h exposure (Figure 2(d)). MBZ activation of ERK1/2 was further confirmed by western blotting (Supplemental Figure 3). MBZ also induced an increase in the M1-phenotype surface markers CD80 and CD86, while there was no change for the M2-phenotype marker CD206, as demonstrated by flow cytometry (Supplemental Figure 4).

Furthermore, using a luminex-based cytokine/chemokine assay, we found that MBZ induced release of pro-inflammatory cytokines IL-1β, TNF, IL17A and IL8, associated with a M1 phenotype (Figure 3(a))²². Moreover, several chemokines, such as MCP-1 (CCL2), MIP-1a (CCL3), MIP-1b (CCL4) and IP-10 (CCL10), were also released in response to MBZ (Figure 3(a)). Compared with LPS, exposure to MBZ caused 5-fold higher increase in IL-1β, whereas the release of TNFα was considerably lower (Figure 3(b,c)). Importantly, no effect on IL-1β release was observed in response to either the benzimidazole compounds FBZ and ABZ or to the tubulin inhibitor vincristine (Supplemental Figure 5).

IL-1β processing and release have been previously associated with P2X receptors²³, which are purinergic ATP-gated cation channels²⁴. Thus, we compared the influence of MBZ and the P2X agonist BzATP on IL-1β gene expression and release, with and without addition of LPS in THP-1 cells. For MBZ used alone, only 6-h exposure to a high concentration (10 μM) caused an increase of IL-1β expression (Figure 4(a–b)) and, consequently, the elevated IL-1β release (measured after 24-h incubation) (Figure 4(c)). As expected, BzATP stimulated IL-1β secretion only when administered together with LPS, which was also the case for a low concentration of MBZ (1 μM). Notably, the addition of LPS to all tested MBZ concentrations caused profound synergistic effect in IL-1β expression and release (Figure 4(a–c)).

To further investigate the underlying cause of pro-inflammatory M1 response of THP-1 cells upon treatment with MBZ, effects of an extended panel of inhibitors of pro-inflammatory signaling pathways were investigated. MBZ-induced IL-1β release was significantly reduced by inhibitors of activation of protein kinase C (Gö6983), MEK (U0126) and NF-κappaB (JSH-23) (Figure 5(a)). Also, oxidized ATP (oATP), an inhibitor of purinergic ligand-gated ATP receptors (such as P2X7), blocked IL-1β secretion (Figure 5(a)). The nonselective

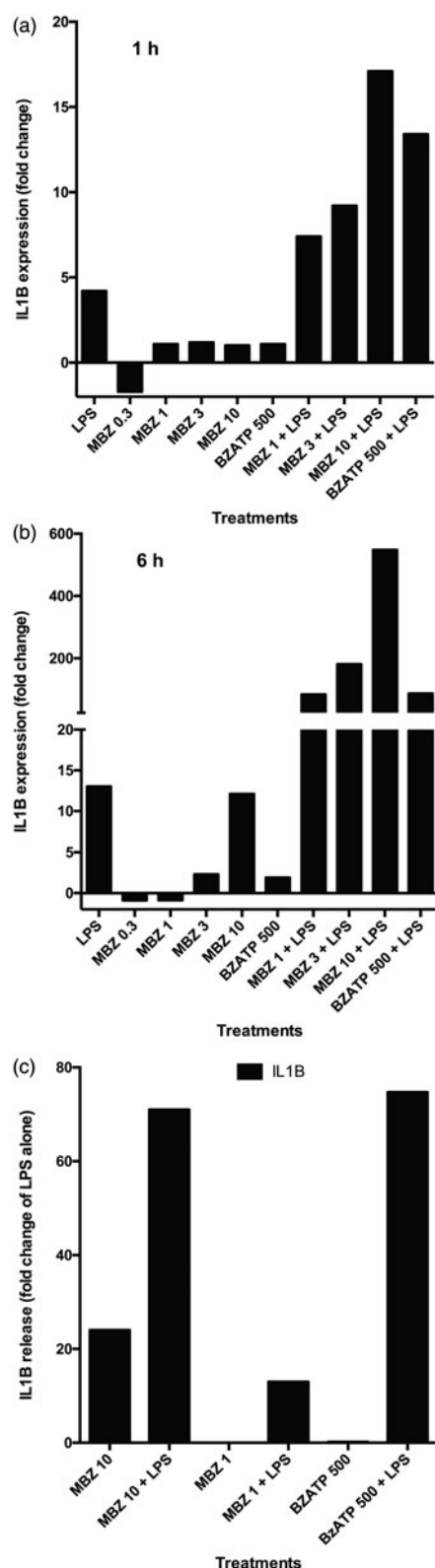


Figure 4. Interaction of MBZ and BzATP with LPS. In (a) and (b), IL-1 β gene expression in response to MBZ or BzATP is shown with and without added LPS after 1 (a) or 6 h (b) of exposure. In (c) IL-1 β release measured 24 h after stimulation with indicated treatments is shown. MBZ strongly potentiated the effect of LPS on IL-1 β gene expression and release.

P2 antagonist suramin showed modest inhibition and KN62, an inhibitor of Ca²⁺/calmodulin-dependent kinase type II, was inactive (Figure 5(a)). IL-1 β secretion strictly requires the assembly and activation of the NOD-like receptor pyrin

domain containing 3 (NLRP3) inflammasome complex²⁵. Since the P2X7 receptor stimulation by ATP is widely implicated in inflammasome activation as a “danger signal”²⁶, we tested its potential involvement using a NLRP3 knock-out THP-1 cell line. The results confirmed that MBZ-induced IL-1 β secretion was significantly reduced in cells lacking the NLRP3 inflammasome (Figure 5(b)). Furthermore, a P2X7-selective antagonist A74003 concentration dependently inhibited MBZ-induced IL-1 β release (Figure 5(c)). However, A74003 was less potent in inhibiting IL-1 β release induced by MBZ than that induced by BzATP (Figure 5(d)). After 24-h exposure, cell viability was >70% for MBZ and all other inhibitors (Supplemental Figure 6). P2X7 stimulation normally leads to a sustained increase in cytoplasmic calcium that is often used as a surrogate marker for monitoring P2X7 activity. However, when measuring the effect of MBZ on cytoplasmic calcium in both THP-1 cells and recombinant P2X7-expressing HEK293 cells, no convincing increase in the fluorescent calcium signal was observed in comparison with DMSO control (Supplemental Figure 7).

The inflammasome activation by P2X7 and other purinergic ATP receptors normally requires an initial activation from stimulation of toll-like receptors (TLRs). To accomplish this in experimental model systems, pretreatment with LPS to induce TLR4-mediated NF-kappaB activation is often performed^{27,28}. However, because TLR7 and TLR8 activation by small molecule agonists such as imiquimod and R848, with some structural resemblance to MBZ²⁹ also can trigger NF-kappaB signaling, we utilized recombinant HEK293 cells overexpressing TLR4, TLR7 or TLR8 to investigate the potential interaction of MBZ with these receptors. While a dose-dependent increase in NF-kappaB activation was observed in the TLR8 overexpressing cells (Figure 5(e)), this was not observed in the TLR7 and TLR4 recombinant cells (Figure 5(f)). As expected, known TLR7/8 (R848, CL075) and seven (imiquimod) agonists activated the NF-kappaB pathway in the TLR8- and TLR7-overexpressing cells, respectively (Figures 5(e–f)). In TLR4 overexpressing cells, only LPS was capable of inducing NF-kappaB activation (Figure 5(f)).

Finally, to study the functional effects of MBZ, we employed a protocol for THP-1 macrophage maturation¹⁸ using phorbol-12-myristate-13-acetate (PMA) treatment (25 ng/mL, 48 h) and further activation (last 18 h) by MBZ (1 and 10 μ M). As positive control, we used LPS (100 ng/mL) and IFN γ (20 ng/mL for the induction of the M1 phenotype and IL4 (20 ng/mL) and IL13 (20 ng/mL) for the M2 phenotype. Compared with PMA treatment only (M0 macrophage generation), addition of MBZ caused a further increase in pro-inflammatory cytokine release with a profile similar to that induced by LPS/IFN γ including a decrease in VEGF release (Supplemental Figure 8). IL4/IL13 treatment showed little increase in pro-inflammatory cytokine release, decreased TNF and caused an increase in VEGF secretion (Supplemental Figure 9). In coculture experiments, we added GFP-labelled colorectal HT-29 and cells to the THP-1 cultures differentiated with PMA followed by activation by LPS/IFN γ (M1), MBZ or IL4/IL13 (M2). The media used for differentiation and activation were washed away before addition of tumor cells. In the

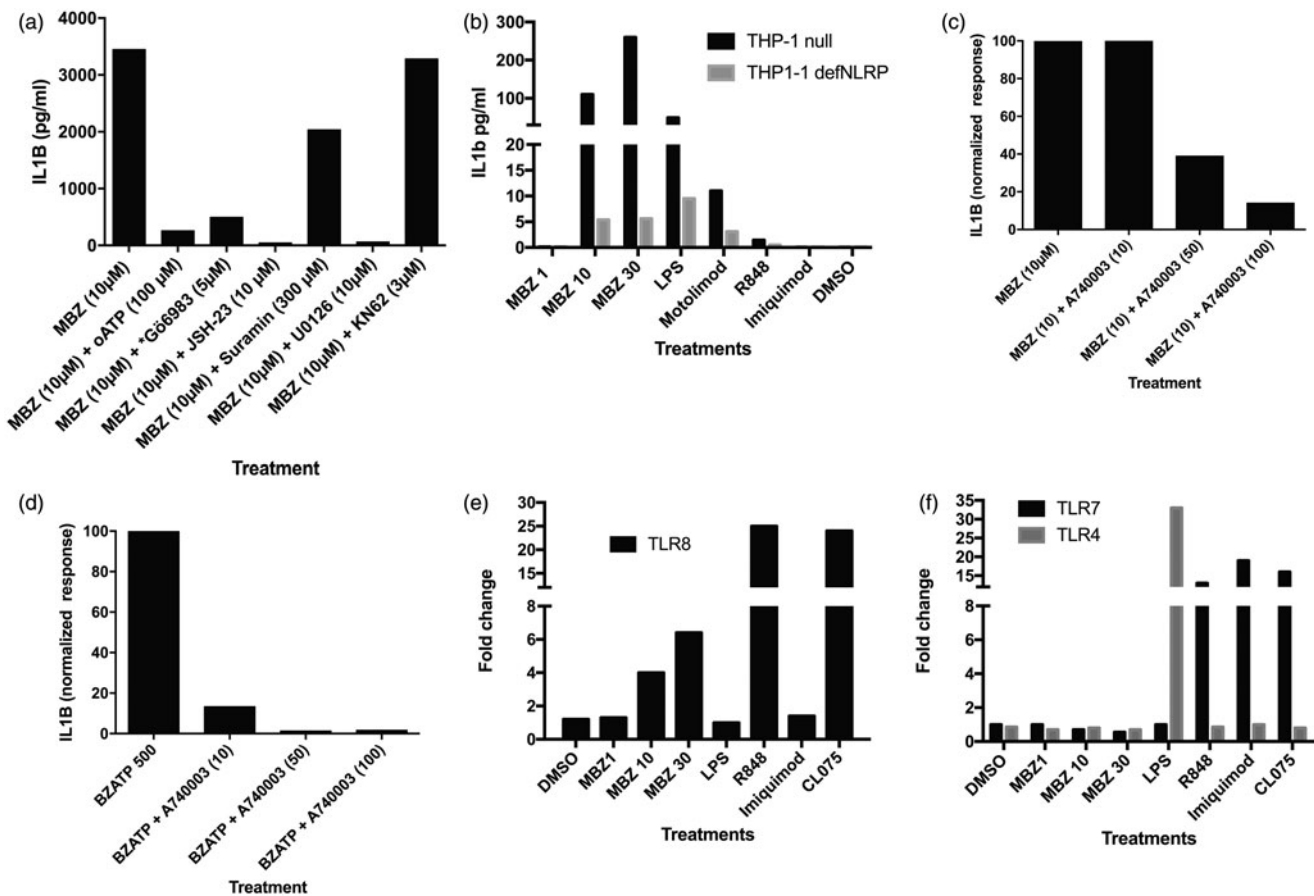


Figure 5. (a) Effect of a panel of specific inhibitors on MBZ-induced IL-1 β release. In (b) IL-1 β secretion in response to MBZ, LPS and TLR7/8 agonists is shown for parental THP-1 cells (black bars) and NLRP3 knock-out cells (grey bars). Panels (c) and (d) shows the effect of the selective P2X7 inhibitor A7004 on MBZ- or BzATP-induced IL-1 β release, respectively. Panels (e) and (f) show the effect of MBZ, LPS and selected TLR7/8 agonists on release of SEAP as a marker for NF-kappaB activation in TLR8- (e), TLR7- and TLR4- overexpressing (f) HEK293 cells and the parental cell line. The increase in NF-kappaB stimulation in response to 10 and 30 μ M MBZ was statistically significant between the TLR8 overexpressing cell line and the parental control ($p < .05$, $n = 3$, Student's t -test). All experiments were repeated at least two times with similar results.

cocultures activated with MBZ or LPS/IFN γ (M1 stimuli), a clear tumor suppressive effect was observed. On the contrary, in cocultures with PMA-differentiated M0 macrophages or those activated by IL4/L13 (M2 stimuli) tumor growth was similar to that observed in tumor cell cultures without THP-1 macrophages (Figure 6).

Discussion

In this study, we first utilized the LINCS database to explore a potential mechanism of action behind anticancer effects of the antihelminthic compound MBZ. An unbiased analysis of existing MBZ gene-expression signatures demonstrated strong negative correlations with MEK and ERK1/2 inhibitors. This was supported by Gene Set Enrichment Analysis and by CMap analysis of MBZ signature from HL60 cells. These results were also supported by a previous publication reporting ERK1/2 activation and stimulated release of IL8 and TNF in response to MBZ³⁰. In this context, it is worth noting that other ERK family members can have overlapping and distinct functions from ERK1/2. For example, ERK5 has been shown to inhibit monocyte to macrophage differentiation³¹. We also demonstrated, using monocytoid THP-1 cells as a model, that

MBZ induces gene expression, surface marker alterations and cytokine release pattern corresponding to a monocyte/macrophage M1 phenotype. Furthermore, MBZ induced tumor suppression in a coculture model with HT-29 colorectal cancer cells and PMA-differentiated THP-1 macrophages. The selection of a colon cancer cell line as target was based on our previous clinical case report¹³.

The monocyte-macrophage system exists in at least two distinct phenotypes of differentiation: pro-inflammatory (M1) and anti-inflammatory (M2)^{18,32}. This functional phenotype plasticity is regulated by local stimuli, such as bacterial LPS or cytokines like IFN γ . The M1 phenotype monocytes/macrophages exhibit phagocytic and antigen-presenting activity, produce Th-1 activating cytokines, and mediate cytotoxic functions, including anticancer activity^{18,32}. The mechanisms by which MBZ-treated THP-1 macrophages induced direct tumor-suppressive effects in HT29 cells is not clear, but the most commonly suggested mechanisms are related to cytokine release (TNF, TRAIL) and/or nitric oxide mediated cell death^{33–36}. The direct cell-killing capabilities of monocytes/macrophages appear to be increased by the M1 stimuli LPS and IFN γ ^{37,38}. Monocytes and macrophages can also promote cytotoxicity indirectly, by activating other cells of the immune system, such as natural killer (NK) and T

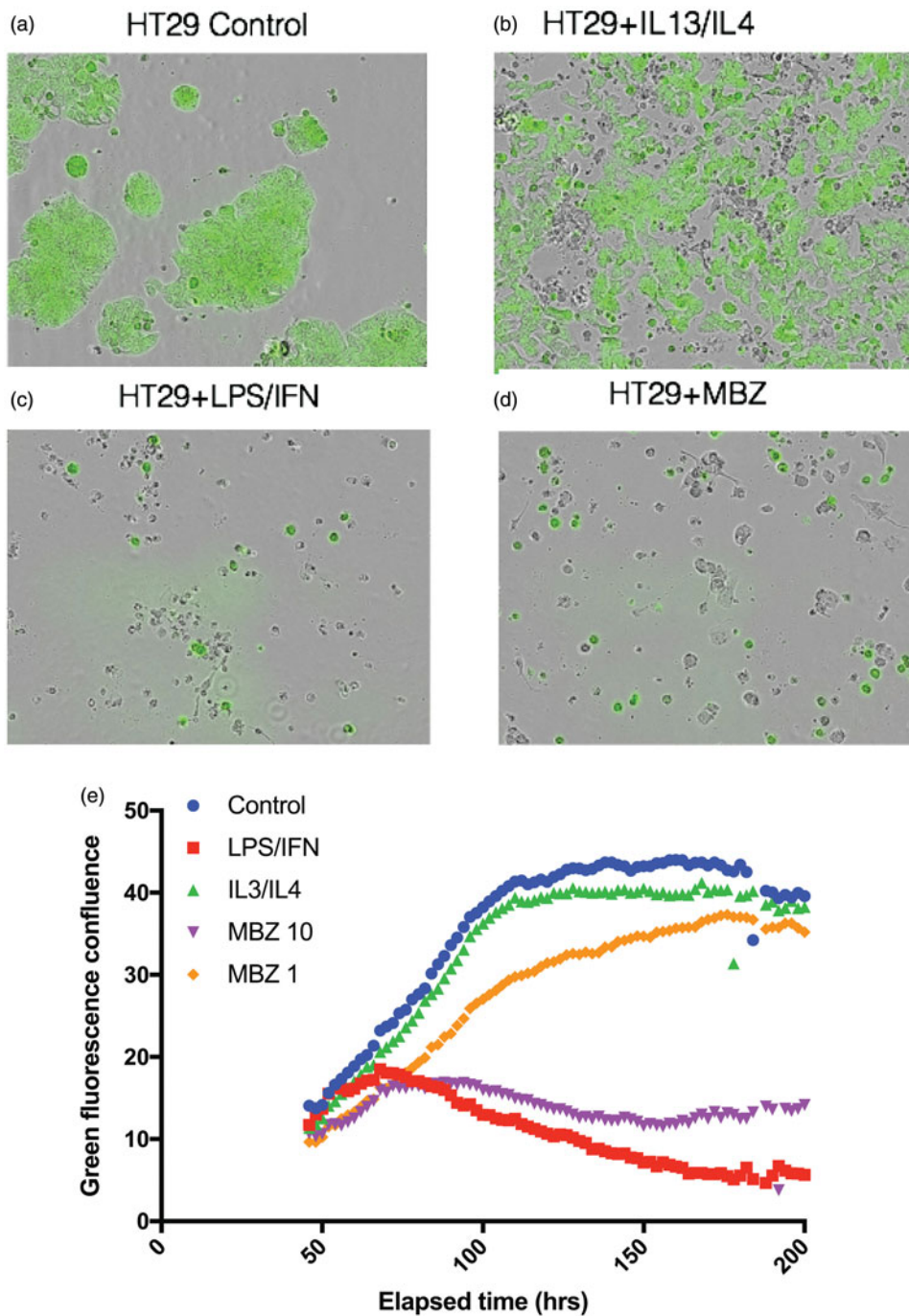


Figure 6. Coculture of PMA-differentiated THP-macrophages and GFP-labeled HT-29 colon cancer cells. THP-1 cells were exposed to PMA (25 ng/mL) for 48 h, followed by an additional stimulation with DMSO, IL4/IL13 (20/20 ng/mL), LPS/IFN (100/20 ng/mL) and MBZ 1 and 10 μ M) for 18 h. After washing away of stimuli-containing media, the HT-29 GFP cells were added and the cultures monitored for 1 week. Representative photomicrographs for the different incubations after 1 week are shown in (a–d), as indicated. The kinetics of changes in green fluorescence (GFP) confluence is presented in (e). The experiment was repeated three times with similar results.

lymphocytes. The M2 macrophages/monocytes, on the other hand, are thought to exert tumor-supporting, angiogenic and immunosuppressive effects^{18,32}. Hence, M2 macrophages play an important role to direct the tumor microenvironment and its architecture to promote the survival and growth of the tumor lesion. Driving macrophages toward an M1 profile with agents such as MBZ could thus hit several pathways stimulating tumor progression and may also support anti-tumor immunity. However, in this context it is also worth noting that chronic inflammation may be carcinogenic³⁹.

IL-1 β is a potent mediator of inflammation and the immune response, produced primarily by activated monocytes^{25,26}. It has been shown to be required to confer an adaptive immune response against tumors by activating antigen-specific CD8 + T-cells⁴⁰. IL-1 β secretion is critically dependent on the assembly and activation of the NLRP3 inflammasome complex²⁵. Activation of the NLRP3 inflammasome has been suggested to require two signals^{27,28}. The first is provided by toll-like-receptor-mediated NF-kappaB activation and triggers the synthesis of the IL-1 β precursor

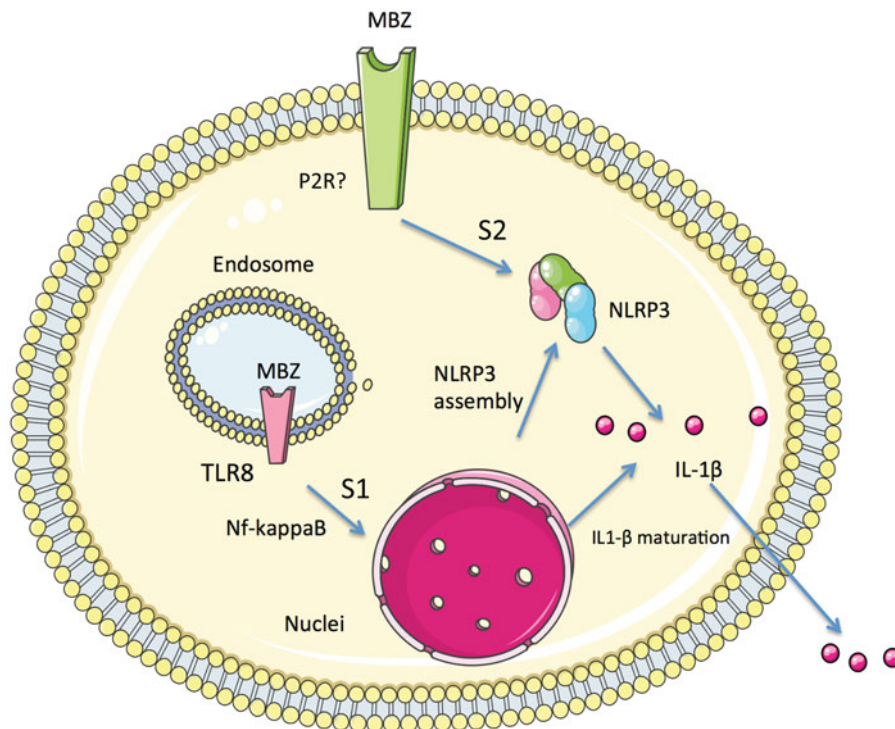


Figure 7. IL-1 β secretion is dependent on the assembly and activation of the NLRP3 inflammasome complex. Activation of the NLRP3 inflammasome has been suggested to require two signals. The first (S1) is provided by toll-like-receptor (TLR)-mediated NF-kappaB activation and triggers the synthesis of the IL-1 β precursor and assembly of NLRP3. The second (S2) can be mediated by danger signals such as stimulation of the purinergic P2X7 receptor by ATP or other stimuli leading to potassium efflux. High dose MBZ (10 μ M) may activate both signals whereas low concentrations (1 μ M) only can activate S2, potentially through purinergic receptors (P2R). High dose MBZ can induce S1 by activating TLR 8.

and assembly of NLRP3. The second can be mediated by danger signals such as stimulation of the purinergic P2X7 receptor by ATP or other stimuli leading to potassium efflux^{26,27,41}. Accordingly, in the present study, MBZ-stimulated IL-1 β gene expression and release was strongly potentiated by concomitant administration with LPS. MBZ at 1 μ M, as well as the P2X7 agonist BzATP, were strictly dependent on LPS for this potentiation to occur. However, at the high concentration (10 μ M), MBZ significantly stimulated IL-1 β release also in the absence of LPS. The explanation for this could involve other TLRs. Indeed, MBZ activated TLR8 at concentrations $\geq 10 \mu$ M. Thus, it seems that at high concentrations MBZ is capable of generating both signals required for IL-1 β release. The potential mechanism for MBZ-induced IL1B is illustrated in Figure 7). Interestingly, a TLR8 agonist, Motilimod (VTX-2337), was recently shown to stimulate the release of mature IL-1 β from monocytic cells through coordinated actions on both TLR8 and the NLRP3 inflammasome complex⁴². VTX-2337-exposed monocytic cells produced pro-IL-1 β , pro-IL-18, and caspase-1 and also activated the NLRP3 inflammasome, thereby mediating the release of mature IL-1 β family cytokines without requiring a second stimuli⁴². This capability was not shared by other TLR7/8 agonists, as also demonstrated in the present study. Notably, VTX-2337 is presently undergoing clinical development for the treatment of solid tumors⁴².

The role of P2X7 in MBZ-induced IL-1 β release, on the other hand, is less clear. Although oATP and the selective P2X7 inhibitor A74003 could inhibit IL-1 β release, no increase in cytoplasmic calcium was observed either in THP1

monocytes or in recombinant P2X7-transfected HEK293 cells. Also, although being reported to be selective for P2X7, A74003 was less potent than BzATP in inhibiting MBZ-induced IL-1 β release. In this context, it should be noted that recombinant P2X7 receptors truncated at the N-terminal lose their ability to activate ERK1/2 without decreasing calcium influx. On the contrary, truncation at the C-terminal, a condition known to abrogate membrane permeabilization (but not cation channel opening), does not affect ERK1/2 activation⁴³. Based on this structural dependency, one can thus speculate that MBZ could selectively activate part of the P2X7 receptor required for ERK1/2 signaling and IL-1 β release. However, the involvement of other P2 receptors mediating these effects cannot be excluded⁴⁴. Furthermore, MBZ induction of danger signals other than NLRP3 inflammasome activation through ATP receptors, such as elevated ROS production or lysosomal cathepsin B release, could potentially contribute to stimulated IL-1 β release⁴⁵. For instance, the TLR8 agonist VTX-2337 has also been suggested to activate the NLRP3 inflammasome through perturbation of lysosome integrity that leads to cathepsin B release⁴².

As for the clinical relevance of the pro-inflammatory properties of MBZ, the drug has been reported to induce objective clinical tumor responses in patients resistant to standard therapy^{12,13}. Notably, a pronounced regression of liver metastases was observed. High-dose treatment with MBZ can result in plasma concentrations close to 1 μ M⁴⁶, a concentration, which in the present study potentiated the immune response, especially IL-1 β release, induced by TLR activation by LPS. However, the concentrations of MBZ in liver tissue

has been reported to be significantly higher than those in plasma probably due to portal venous uptake and biliary excretion⁴⁶. Consequently, high MBZ concentration in the liver might trigger M1-polarization of tumor-associated macrophages and/or DCs. This, in turn, could lead to a pro-inflammatory and adaptive immune response against the liver metastases and subsequently result in a systemic anti-cancer effect. However, the potential role of MBZ in cancer therapy has yet to be determined in ongoing and future clinical trials.

In summary, we here report that MBZ induces a M1 phenotype and mapped the cellular transmission signals for this effect. Our observations may at least partly explain the MBZ induced anticancer effects observed *in vivo*. Since M2 macrophages drive tumor progression, it is of high interest to find agents that may shift the tumor microenvironment to harbor M1 macrophages and to release T cell chemoattractants. MBZ with its favorable safety profile may be an attractive alternative, especially for patients with liver metastases.

Acknowledgements

We thank In Vitro and Systems Pharmacology facility of the Science for Life Laboratory for helpful assistance. The study was supported by the Swedish Cancer Society and the Lions Cancer Research Fund.

Disclosure statement

RL, PN and MF are co-founders and shareholders of Repos Pharma AB, a small Swedish research and development company dedicated to investigations of drug repositioning in the cancer area. AL is chairman of the board. The present work were funded only by academic grants. The remaining authors declare no conflict of interest.

Funding

The study was supported by the Swedish Cancer Society and the Lions Cancer Research Fund.

ORCID

Rolf Larsson  <http://orcid.org/0000-0002-3427-4128>

References

- Pantziarka P, Bouche G, Meheus L, et al. Repurposing drugs in oncology (ReDO)-mebendazole as an anti-cancer agent. *Ecancermedalscience* 2014;8:443.
- Doudican N, Rodriguez A, Osman I, Orlow SJ. Mebendazole induces apoptosis via Bcl-2 inactivation in chemoresistant melanoma cells. *Mol Cancer Res* 2008;6:1308–1315.
- Bai R-Y, Staedtke V, Aprhys CM, et al. Antiparasitic mebendazole shows survival benefit in 2 preclinical models of glioblastoma multiforme. *Neuro-Oncol* 2011;13:974–982.
- Sasaki JI, Ramesh R, Chada S, et al. The anthelmintic drug mebendazole induces mitotic arrest and apoptosis by depolymerizing tubulin in non-small cell lung cancer cells. *Mol Cancer Ther* 2002;1:1201–1209.
- Martarelli D, Pompei P, Baldi C, Mazzoni G. Mebendazole inhibits growth of human adrenocortical carcinoma cell lines implanted in nude mice. *Cancer Chemother Pharmacol* 2008;61:809–817.
- Mukhopadhyay T, Sasaki JI, Ramesh R, Roth JA. Mebendazole elicits a potent antitumor effect on human cancer cell lines both *in vitro* and *in vivo*. *Clin Cancer Res* 2002;8:2963–2969.
- Nygren P, Fryknäs M, Agerup B, Larsson R. Repositioning of the anthelmintic drug mebendazole for the treatment of colon cancer. *J Cancer Res Clin Oncol* 2013;139:2133–2140.
- Doudican NA, Byron SA, Pollock PM, Orlow SJ. XIAP downregulation accompanies mebendazole growth inhibition in melanoma xenografts. *Anticancer Drugs* 2013;24:181–188.
- Bai R-Y, Staedtke V, Rudin CM, et al. Effective treatment of diverse medulloblastoma models with mebendazole and its impact on tumor angiogenesis. *Neuro-Oncol* 2014.
- Bodhinayake I, Symons M, Boockvar JA. Repurposing mebendazole for the treatment of medulloblastoma. *Neurosurgery* 2015;76:N15–N16.
- Pinto LC, Pinheiro J, de JV, Burbano RMR. The anthelmintic drug mebendazole inhibits growth, migration and invasion in gastric cancer cell model. *Toxicol In Vitro* 2015;29:2038–2044.
- Dobrosotskaya IY, Hammer GD, Schteingart DE, et al. Mebendazole monotherapy and long-term disease control in metastatic adrenocortical carcinoma. *Endocr Pract* 2011;17:e59–e62.
- Larsson R, Nygren P. Drug repositioning from bench to bedside: Tumour remission by the anthelmintic drug mebendazole in refractory metastatic colon cancer. *Acta Oncol* 2013;53:1–2.
- Larsen AR, Bai RY, Chung JH, et al. Repurposing the anthelmintic mebendazole as a hedgehog inhibitor. *Mol Cancer Ther* 2015;14:3–13.
- Bai RY, Staedtke V, Wanjiku T, et al. Brain penetration and efficacy of different mebendazole polymorphs in a mouse brain tumor model. *Clin Cancer Res* 2015;21:3462–3470.
- Brennan RJ, Nikolskya T, Bureeva S. Network and pathway analysis of compound-protein interactions. *Methods Mol Biol* 2009;575:225–247.
- Lindhagen E, Nygren P, Larsson R. The fluorometric microculture cytotoxicity assay. *Nat Protoc* 2008;3:1364–1369.
- Stewart DA, Yang Y, Makowski L, Troester MA. Basal-like breast cancer cells induce phenotypic and genomic changes in macrophages. *Mol Cancer Res* 2012;10:727–738.
- Aricò E, Wang E, Tornesello ML, et al. Immature monocyte derived dendritic cells gene expression profile in response to virus-like particles stimulation. *J Transl Med* 2005;3:45.
- Kurihara Y, Nakahara T, Furue M. $\alpha V\beta 3$ -integrin expression through ERK activation mediates cell attachment and is necessary for production of tumor necrosis factor alpha in monocytic THP-1 cells stimulated by phorbol myristate acetate. *Cell Immunol* 2011;270:25–31.
- Chanput W, Mes JJ, Wichers HJ. THP-1 cell line: an *in vitro* cell model for immune modulation approach. *Int Immunopharmacol* 2014;23:37–45.
- Biswas SK, Mantovani A. Macrophage plasticity and interaction with lymphocyte subsets: cancer as a paradigm. *Nat Immunol* 2010;11:889–896.
- Gabel CA. P2 purinergic receptor modulation of cytokine production. *Purinergic Signal* 2007;3:27–38.
- Di Virgilio F, Vuerich M. Purinergic signaling in the immune system. *Auton Neurosci* 2015;191:117–123.
- Gicquel T, Robert S, Loyer P, et al. IL-1 β production is dependent of the activation of purinergic receptors and NLRP3 pathway in human macrophages. *Faseb J* 2015;29:4162–4173.
- Ward JR, West PW, Ariaans MP, et al. Temporal interleukin-1 β secretion from primary human peripheral blood monocytes by P2X7-independent and P2X7-dependent mechanisms. *J Biol Chem* 2010;285:23147–23158.
- Wewers MD, Sarkar A. P2X(7) receptor and macrophage function. *Purinergic Signal* 2009;5:189–195.
- Ghonime MG, Shamaa OR, Das S, et al. Inflammasome priming by lipopolysaccharide is dependent upon ERK signaling and proteasome function. *J Immunol* 2014;192:3881–3888.
- Schön MP. TLR7 and TLR8 as targets in cancer therapy. *Oncogene* 2008;27:190–199.

30. Mizuno K, Toyoda Y, Fukami T, et al. Stimulation of pro-inflammatory responses by mebendazole in human monocytic THP-1 cells through an ERK signaling pathway. *Arch Toxicol* 2011;85:199–207.
31. Wang X, Pesakhov S, Harrison JS, et al. The MAPK ERK5, but not ERK1/2, inhibits the progression of monocytic phenotype to the functioning macrophage. *Exp Cell Res* 2015;330:199–211.
32. Panni RZ, Linehan DC, DeNardo DG. Targeting tumor-infiltrating macrophages to combat cancer. *Immunotherapy* 2013;5:1075–1087.
33. Williams MA, Newland AC, Kelsey SM. The potential for monocyte-mediated immunotherapy during infection and malignancy. Part I: apoptosis induction and cytotoxic mechanisms. *Leuk Lymphoma* 1999;34:1–23.
34. Klostergaard J. Macrophage tumoricidal mechanisms. *Res Immunol* 1993;144:274–276.
35. Cui S, Reichner JS, Mateo RB, Albina JE. Activated murine macrophages induce apoptosis in tumor cells through nitric oxide-dependent or -independent mechanisms. *Cancer Res* 1994;54:2462–2467.
36. Griffith TS, Wiley SR, Kubin MZ, et al. Monocyte-mediated tumoricidal activity via the tumor necrosis factor-related cytokine, TRAIL. *J Exp Med* 1999;189:1343–1354.
37. Cameron DJ, Churchill WH. Cytotoxicity of human macrophages for tumor cells: enhancement by bacterial lipopolysaccharides (LPS). *J Immunol* 1980;124:708–712.
38. Chen GG, Lau WY, Lai PBS, et al. Activation of Kupffer cells inhibits tumor growth in a murine model system. *Int J Cancer* 2002;99:713–720.
39. Mantovani A, Allavena P, Sica A, Balkwill F. Cancer-related inflammation. *Nature* 2008;454:436–444.
40. Ghiringhelli F, Apetoh L, Tesniere A, et al. Activation of the NLRP3 inflammasome in dendritic cells induces IL-1beta-dependent adaptive immunity against tumors. *Nat Med* 2009;15:1170–1178.
41. Muñoz-Planillo R, Kuffa P, Martínez-Colón G, et al. K⁺ efflux is the common trigger of NLRP3 inflammasome activation by bacterial toxins and particulate matter. *Immunity* 2013;38:1142–1153.
42. Dietsch GN, Lu H, Yang Y, et al. Coordinated activation of toll-like receptor8 (TLR8) and NLRP3 by the TLR8 agonist, VTX-2337, ignites tumoricidal natural killer cell activity. *PLoS One* 2016;11:e0148764–e0148718.
43. Amstrup J, Novak I. P2X7 receptor activates extracellular signal-regulated kinases ERK1 and ERK2 independently of Ca²⁺ influx. *Biochem J* 2003;374:51–61.
44. da Cruz CM, Ventura ALM, Schachter J, et al. Activation of ERK1/2 by extracellular nucleotides in macrophages is mediated by multiple P2 receptors independently of P2X7-associated pore or channel formation. *Br J Pharmacol* 2006;147:324–334.
45. Franchi L, Muñoz-Planillo R, Núñez G. Sensing and reacting to microbes through the inflammasomes. *Nat Immunol* 2012;13:325–332.
46. Braithwaite PA, Roberts MS, Allan RJ, Watson TR. Clinical pharmacokinetics of high dose mebendazole in patients treated for cystic hydatid disease. *Eur J Clin Pharmacol* 1982;22:161–169.